

# A MICROBUBBLE PRESSURE TRANSDUCER WITH BUBBLE NUCLEATION CORE

Lawrence Yu and Ellis Meng

University of Southern California, Los Angeles, USA

## ABSTRACT

A microchannel-based microbubble ( $\mu$ B) transducer ( $\mu$ BPT) having a  $\mu$ B nucleation core ( $\mu$ BNC) was developed to achieve low power operation in wet environments. In this work, we investigate  $\mu$ B dynamics within the transducer structure and pressure transduction. The transducer leverages electrochemical impedance (EI)-based measurement to monitor the instantaneous response of  $\mu$ B size changes induced by hydrostatic pressure changes. We demonstrated on-demand  $\mu$ B nucleation by electrolysis and real-time pressure tracking ( $-93 \Omega/\text{mmHg}$  over  $0\text{-}350 \text{ mmHg}$ ). Repeatable, efficient electrolytic generation of stable microbubbles ( $< 1.5 \text{ nL}$  with  $< 2\%$  size variation) was achieved using a  $\mu$ BNC structure attached centrally to the microchannel. Biocompatible construction (only Parylene and Pt), small footprint, low power consumption ( $< 60 \mu\text{W}$ ), and liquid-based operation of  $\mu$ BPTs are ideal for *in vivo* pressure monitoring applications.

## INTRODUCTION

Typically MEMS pressure transducers consist of a flexible diaphragm affixed to a stiffer supporting structure. Such a structure conveniently utilizes capacitive or piezoelectric transduction mechanisms. Here, we employ an alternative approach which exploits the ability of a microbubble to respond instantaneously to external pressure variations [1]. By combining localization of a microbubble with electrochemical transduction, our pressure transduction approach obviates the need for hermetic packaging required of conventional pressure sensor structures when used for *in vivo* monitoring and thereby significantly reduces the overall sensor footprint.

## DESIGN

### Transduction Principle

Previously, pressure response of  $\mu$ Bs generated within silicon microfluidic channels was investigated [2] but with poor control over the repeatability during electrolytic bubble nucleation ( $> 6\%$  size variation). We developed a  $\mu$ BPT based on a circular Parylene chamber and flexible substrate but achieved limited sensitivity due to the short EI measurement path. Also, the electrolysis/measurement electrodes were shared and thus switching was required for sensor operation [3]. Electrode spacing for optimal electrolytic nucleation and EI measurement have opposing requirements: increased spacing between electrodes results in a larger measurement range while closely spaced electrodes enables localized bubble formation. Therefore, to improve sensitivity for *in vivo* applications, the use of distinct pairs of smaller area electrodes for electrolysis

residing in a separate structure (a  $\mu$ BNC) and larger area electrodes for high precision EI measurement was investigated (Fig. 1).

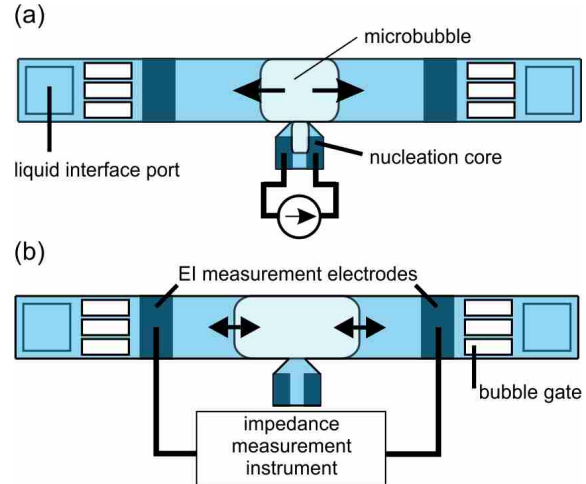


Figure 1: Top-down illustration of pressure transduction principle and layout of pressure transducer. (a) Microbubbles are electrolytically generated within a nucleation core and coalesce into a single bubble. The growing bubble extends outwards and fills measurement region of the channel. (b) The  $\mu$ B then detaches from the  $\mu$ BNC and remains in the measurement channel where it can respond to local pressure changes transmitted via the liquid interface ports.

In order to perform a pressure measurement, first a  $\mu$ B is formed via electrolysis in the nucleation core and enters the measurement channel as it grows (Fig. 1a), forming capillaries of fluid in the channel corners (Fig. 2). Once a sufficient size is reached, electrolysis current is terminated and the  $\mu$ B detaches from the nucleation core. The electrically insulating bubble now resides in the measurement channel region and is available for pressure transduction (Fig 1b). A low power, high frequency alternating current applied across the EI measurement electrodes permits monitoring of the volumetric conductive path (solution resistance  $R_s$  in Fig. 3) [4]. External pressure of the liquid media is transferred through the interface ports (Fig. 1a), which directly influences bubble size. These pressure variations induce  $\mu$ B size changes that are reflected in the measured impedance,  $Z$ :

$$|Z|_{f \geq 10\text{kHz}} \approx R_s = \frac{\rho\ell}{s_{Tot}} \quad (1)$$

where  $R_s$  is solution resistance,  $\rho$  is conductivity of

electrolyte,  $\ell$  is the length of the fluid capillary formed by a  $\mu$ B residing in the microchannel, and

$$S_{Tot} = 4 \frac{r^2}{R^2} \left[ \frac{\cos \theta}{\sin \pi/4} \cos(\pi/4 + \theta) - (\pi/4 - \theta) \right] \quad (2)$$

$R$  is the inscribed inner radius of the channel,  $r$  the radius of curvature of the corner meniscus, and  $\theta$  the contact angle of the  $\mu$ B with the channel wall (Fig. 3) [2].

This conductive path geometry improves sensitivity over our previous design by leveraging the large changes in impedance observed in submicron fluid capillaries [5].

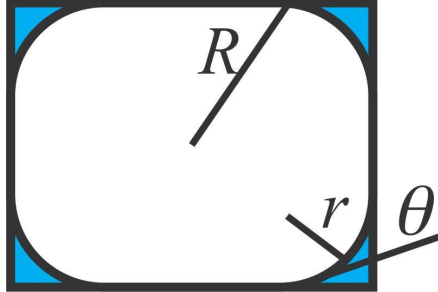


Figure 2: Cross sectional view of bubble in microchannel in measurement region. Capillaries of fluid (shown in blue) reside in corners between the bubble boundary and channel walls. Total cross sectional area ( $S_{Tot}$ ) of conductive fluid capillary path is dependent on contact angle of channel sidewall material.

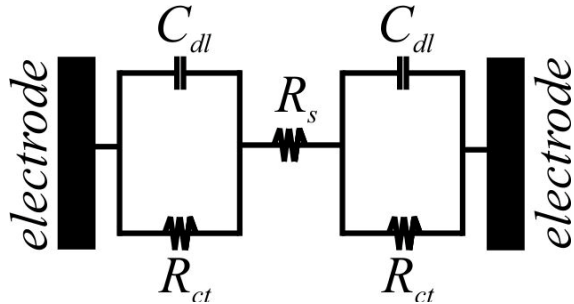


Figure 3: Impedance between measurement electrodes modeled by the Randles circuit is proportional to length of microbubble in measurement channel.

### Nucleation Core

The  $\mu$ BNC consists of a pair of closely-spaced microelectrodes (50  $\mu$ m apart) enclosed within a tapered cavity shaped so as to direct bubbles into the adjacent microchannel. Typically, nucleation via electrolysis creates  $\mu$ Bs within natural microcavities randomly distributed on the electrode surface [6]; the cavity structure of the  $\mu$ BNC forces  $\mu$ Bs to coalesce before entering the microchannel. When the  $\mu$ B spans the width of the microchannel, surface energy of the hydrophobic Parylene sidewall causes the bubble to adhere, and termination of electrolysis current results in  $\mu$ B detachment from the  $\mu$ BNC. Thus, a single bubble is generated and localized in the measurement area.

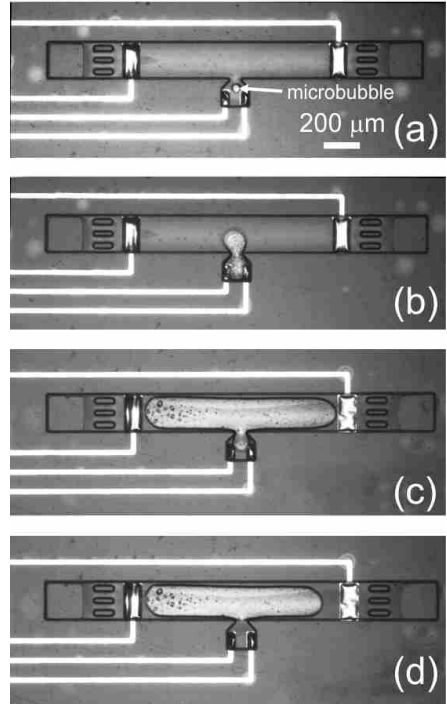


Figure 4: Bubble nucleation and formation process. (a) Nucleation via electrolysis in  $\mu$ B nucleation core. (b)  $\mu$ B enters measurement channel. (c) Continued growth fills microchannel. (d) Detachment of  $\mu$ B from  $\mu$ BNC and localization in the measurement channel.

### Microchannel Measurement Area

A microchannel serves to confine the  $\mu$ B and provide an area for EI measurements. Gating structures in the microchannel keep  $\mu$ Bs within the measurement area and prevent escape through the open-ended channels. Situating the  $\mu$ BNC between and equidistant from the measurement microelectrodes located at the ends of the microchannel maximizes area for  $\mu$ B growth, thus maximizing measurement range.

## METHODS

### Fabrication

The  $\mu$ BPT was fabricated (Fig. 5) on a flexible Parylene C substrate with thin film Pt electrodes based on previously reported techniques [7]. Platinum was deposited (2000 Å thick) and patterned on a Parylene coated (10  $\mu$ m thick) silicon wafer. Following deposition of a 2  $\mu$ m Parylene insulation layer, sacrificial photoresist was patterned to establish the microchannel and  $\mu$ BNC structures. A final 2  $\mu$ m thick layer of Parylene was used to enclose the structure, and access ports were patterned and opened with oxygen plasma.

Devices were released in an acetone bath, and an electrical connection was established with a ZIF connector, using previously reported methods [8]. The microchannel was first soaked in isopropyl alcohol to facilitate filling with 1X PBS, the measurement solution.

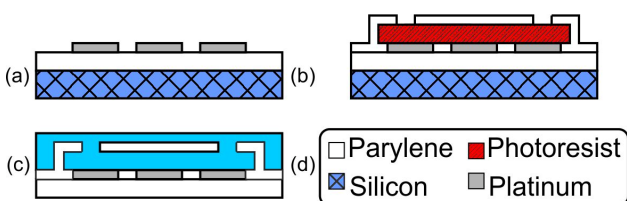


**Figure 5:** Overview of transducer microfabrication process. (a) Deposit 1<sup>st</sup> Parylene and perform Pt lift-off. (b) Pattern sacrificial photoresist, deposit 2<sup>nd</sup> Parylene layer, and etch interface ports. (c) Release device from silicon substrate and soak in electrolyte to fill channel.

### Experimental Setup

Microbubbles were electrolytically generated (Fig. 4) in 1X PBS under LabVIEW control over 1-4  $\mu$ A for 5-25 s at the  $\mu$ BNC and consistently exited into the measurement channel. During current injection, multiplexed impedance measurements were taken (Fig. 6) with a precision LCR meter (Agilent E4980A). Bubble size was quantified optically and with EI measurement. Electrochemical impedance spectroscopy (EIS) yielded 10 kHz as the optimum frequency (minimum system phase) for maximizing the solution resistance component of the impedance response (Fig. 7). Hydrostatic pressure measurement used a calibrated pressure source attached to a custom test fixture housing the  $\mu$ BPT. A  $\mu$ B was generated at 0 mmHg and subsequent pressure oscillations were tracked in real-time (Fig. 9).

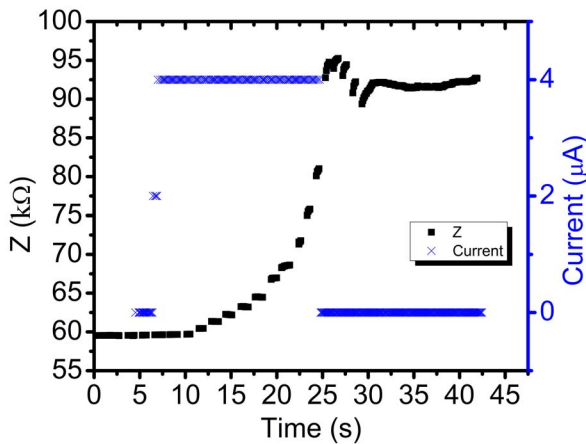


**Figure 6:** Impedance tracking of bubble nucleation in 1X PBS superimposed on the injected current pulse.

## RESULTS AND DISCUSSION

Localized and metered bubble nucleation was repeatable. Power draw was  $\sim$ 1 nW for EI measurement ( $1V_{p-p}$ ) and  $< 60 \mu$ W for electrolytic bubble generation. Impedance monitoring during  $\mu$ B nucleation enabled precise control of bubble formation, and this rate is hypothesized to be correlated to the hydrostatic pressure [9].

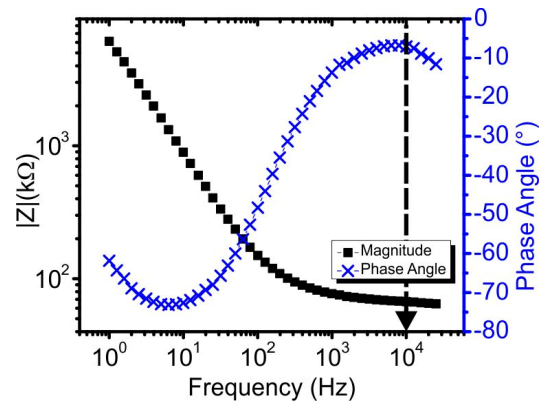


**Figure 7:** Magnitude and phase for measurement electrodes in 1X PBS. To eliminate capacitive effects, measurement frequency was selected where phase  $\sim 0^\circ$  (10 kHz).

Three types of  $\mu$ Bs were observed (Fig. 8): type I  $\mu$ Bs were confined in the  $\mu$ BNC (Fig. 4a,  $< 16 \mu$ C); type II (Fig. 4b) spanned both the  $\mu$ BNC and microchannel (16-40  $\mu$ C); type III (Fig. 4c) resided in the microchannel, detached (Fig. 4d) from the  $\mu$ BNC ( $> 40 \mu$ C). Bubble type can be categorized based on the total injected charge during electrolysis. Pressure transduction was performed only with type III  $\mu$ Bs. The gas evolved from electrolysis of PBS is nearly all hydrogen [10], resulting in the short lifetime ( $< 5$  s) of type I and II  $\mu$ Bs due to  $H_2$  contact with Pt electrodes, which catalyze recombination. Type III  $\mu$ Bs maintained constant size ( $> 15$  min) due to diffusion-limited dissolution (Fig. 6; partial time course shown). High precision EI measurement (SD  $< 2\%$ ) of bubble size was achieved.

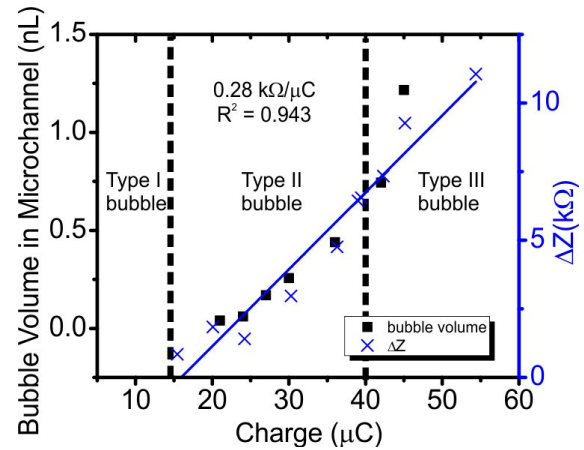


**Figure 8:** Metered current injection for  $\mu$ B nucleation correlates to a change in impedance. Dashed lines distinguish bubble morphologies based on injected charge.

A linear trend between EI and applied pressure was observed (Fig. 9), suggesting bubble length is proportional to applied pressure as described in Eq 1. For the same measurement range, sensitivity was improved three orders of magnitude compared to the previous circular chamber design ( $0.22\Omega/\text{mmHg}$ ); this improvement is attributed to the

high impedance response of the submicron fluid capillaries.

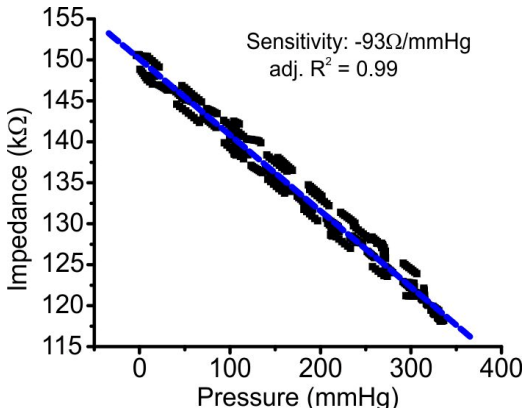


Figure 9: Impedance-pressure correlation for Type III  $\mu$ Bs. Obtained highly linear response with improved sensitivity compared to previous chamber design.

On a type III  $\mu$ B, pressure oscillations were tracked in real-time (Fig. 10). Dissolution of the bubble was relatively slow and dependent on mass transport and interfacial kinetics, enabling stable pressure tracking measurement for an adequate time period ( $> 15$  min). Bubble detachment from the  $\mu$ BNC also favors the slow diffusion-limited process over the Pt-catalyzed recombination reaction.

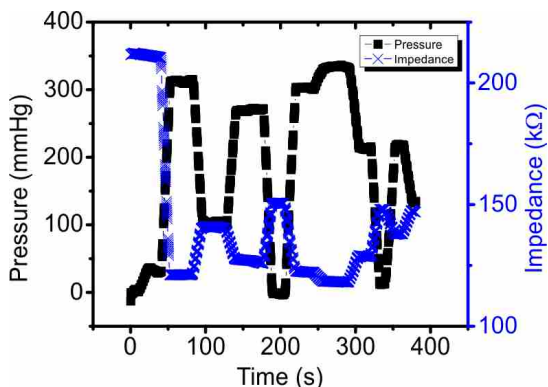


Figure 10: Real-time pressure tracking with type III microbubble.

## CONCLUSIONS

Precise control of  $\mu$ B formation is essential in pressure transduction based on  $\mu$ B response to pressure variations. The use of a  $\mu$ BNC structure for high precision  $\mu$ B nucleation and pressure tracking using the localized  $\mu$ B in an adjacent microchannel was demonstrated. Generated  $\mu$ Bs were stable ( $> 15$  min) and the new sensor geometry allowed improved sensitivity over the previous circular chamber design. Further sensor characterization under varying environments (electrolyte composition, temperature, and pH) is underway.

## ACKNOWLEDGEMENTS

This work was funded by the NSF under award number

ECCS-1231994. The authors would like to thank Mr. J. Nishida, Mr. A. Jibodu, and the members of the USC Biomedical Microsystems Laboratory for their assistance.

## REFERENCES

- [1] P. S. Epstein and M. S. Plesset, "On the Stability of Gas Bubbles in Liquid-Gas Solutions," *Journal of Chemical Physics*, vol. 18, pp. 1505-1509, 1950.
- [2] D. A. Ateya, A. A. Shah, and S. Z. Hua, "Impedance-based response of an electrolytic gas bubble to pressure in microfluidic channels," *Sensors and Actuators, A: Physical*, vol. 122, pp. 235-241, 2005.
- [3] C. A. Gutierrez and E. Meng, "A subnanowatt microbubble pressure sensor based on electrochemical impedance transduction in a flexible all-parylene package," in *24th IEEE International Conference on Micro Electro Mechanical Systems, MEMS 2011, January 23, 2011 - January 27, 2011, Cancun, Mexico, 2011*, pp. 549-552.
- [4] J. E. B. Randles, "Kinetics of Rapid Electrode Reactions," *Discussions of the Faraday Society*, vol. 1, pp. 11-19, 1947.
- [5] D. A. Ateya, A. A. Shah, S. Z. Hua, and F. Sachs, "Bubble based microfluidic sensors," in *2004 ASME International Mechanical Engineering Congress and Exposition, IMECE 2004, November 13, 2004 - November 19, 2004, Anaheim, CA, United states, 2004*, pp. 437-441.
- [6] A. Volanschi, D. Oudejans, W. Olthuis, and P. Bergveld, "Gas phase nucleation core electrodes for the electrolytical method of measuring the dynamic surface tension in aqueous solutions," in *Sixth International Meeting on Chemical Sensors, 22-25 July 1996, Switzerland, 1996*, pp. 73-9.
- [7] C. A. Gutierrez, C. McCarty, B. Kim, M. Pahwa, and E. Meng, "An Implantable All-Parylene Liquid-Impedance Based MEMS Force Sensor," in *MEMS 2010: 23rd IEEE International Conference on Micro Electro Mechanical Systems, Technical Digest*, ed New York: IEEE, 2010, pp. 600-603.
- [8] B. J. Kim, C. A. Gutierrez, G. A. Gerhardt, and E. Meng, "Parylene-based electrochemical-MEMS force sensor array for assessing neural probe insertion mechanics," in *Micro Electro Mechanical Systems (MEMS), 2012 IEEE 25th International Conference on*, 2012, pp. 124-127.
- [9] N. P. Brandon and G. H. Kelsall, "Growth kinetics of bubbles electrogenerated at microelectrodes," *Journal of Applied Electrochemistry*, vol. 15, pp. 475-484, 1985/07/01 1985.
- [10] S. Z. Hua, F. Sachs, D. X. Yang, and H. D. Chopra, "Microfluidic Actuation Using Electrochemically Generated Bubbles," *Analytical Chemistry*, vol. 74, pp. 6392-6396, 2002/12/01 2002.

## CONTACT

\*E. Meng, tel: +1-213-8213949; ellis.meng@usc.edu